Atmospheric
Chemistry
and Physics

Causes of growing middle-to-upper tropospheric ozone over the northwest Pacific region

Xiaodan Ma[1,2], **Jianping Huang**[3,4], **Michaela I. Hegglin**[2,5], **Patrick Jöckel**[6], and **Tianliang Zhao**[1]

[1]Collaborative Innovation Center on Forecast and Evaluation of Meteorological Disasters, Key Laboratory for Aerosol-Cloud-Precipitation of China Meteorological Administration, Nanjing University of Information Science and Technology, Nanjing 210044, China
[2]Institute of Energy and Climate Research – Stratosphere (IEK-7), Forschungszentrum Jülich, Jülich, Germany
[3]Environmental Modeling Center, NOAA National Centers for Environmental Prediction, College Park, MD, USA
[4]Center for Spatial Information Science and Systems, College of Science, George Mason University, Fairfax, VA 22030, USA
[5]Department of Meteorology, University of Reading, Reading, United Kingdom
[6]Deutsches Zentrum für Luft- und Raumfahrt (DLR), Institut für Physik der Atmosphäre, Oberpfaffenhofen, Germany

Correspondence: Jianping Huang (jianping.huang@noaa.gov)

Abstract. Long-term ozone (O_3) changes in the middle-to-upper troposphere are critical to climate radiative forcing and tropospheric O_3 pollution. Yet, these changes remain poorly quantified through observations in East Asia. Concerns also persist regarding the data quality of the ozonesondes available at the World Ozone and Ultraviolet Radiation Data Centre (WOUDC) for this region. This study aims to address these gaps by analyzing O_3 soundings at four sites along the northwestern Pacific coastal region over the past 3 decades and by assessing their consistency with an atmospheric chemistry–climate model simulation. Utilizing the European Centre for Medium-Range Weather Forecasts (ECMWF) Hamburg (ECHAM)/Modular Earth Submodel System (MESSy) Atmospheric Chemistry (EMAC) nudged simulations, it is demonstrated that trends between model and ozonesonde measurements are overall consistent, thereby gaining confidence in the model's ability to simulate O_3 trends and confirming the utility of potentially imperfect observational data. A notable increase in O_3 mixing ratio around 0.29–0.82 ppb a^{-1} extending from the middle troposphere to the upper troposphere is observed in both observations and model simulations between 1990 and 2020, primarily during spring and summer. The timing of these O_3 tongues is delayed when moving from south to north along the measurement sites, transitioning from late spring to summer. Investigation into the drivers of these trends using tagged model tracers reveals that O_3 of stratospheric origin (O_3S) dominates the absolute O_3 mixing ratios over the middle-to-upper troposphere in the subtropics, contributing to the observed O_3 increases by up to 96 % (40 %) during winter (summer), whereas O_3 of tropospheric origin (O_3T) governs the absolute value throughout the tropical troposphere and contributes generally much more than 60 % to the positive O_3 changes, especially during summer and autumn. During winter and spring, a decrease in O_3S is partly counterbalanced by an increase in O_3T in the tropical troposphere. This study highlights that the enhanced downward transport of stratospheric O_3 into the troposphere in the subtropics and a surge of tropospheric O_3 in the tropics are the two key factors driving the enhancement of O_3 in the middle-to-upper troposphere along the northwest Pacific region.

1 Introduction

Stratospheric intrusions and photochemical production are two major contributors to tropospheric ozone (O_3; Ding and Wang, 2006; Neu et al., 2014; Williams et al., 2019; Zhao et al., 2021). The stratosphere accommodates 90 % of the total O_3 in the atmosphere. As the largest natural source, downward transport of O_3-enriched air from the stratosphere exerts an important impact particularly on the seasonality of tropospheric O_3 (Williams et al., 2019). Free tropospheric O_3 increases of 7 % (measured as a partial column between 3–9 km) between 2005 and 2010 over China have been identified as a consequence of increased O_3 precursor emissions and enhanced downward transport from stratospheric O_3 (Verstraeten et al., 2015). While photochemical production is highly dependent on anthropogenic emissions, the impact of stratospheric intrusions on tropospheric O_3 is mainly governed by interannual variability and climate-driven changes in the atmospheric circulation (Neu et al., 2014; Albers et al., 2018). Compared to the spatiotemporal variations of O_3 in the lower troposphere, the evolution in the middle-to-upper troposphere and their underlying causes remain inadequately quantified, largely due to scarcity of long-term, vertically resolved observational data.

Chemistry–climate modeling studies demonstrate that climate variability in the atmospheric circulation, such as an enhanced Brewer–Dobson circulation (BDC), can promote greater seasonal buildup of O_3 in the extratropical lowermost stratosphere during winter (Ray et al., 1999; Sudo et al., 2003; Konopka et al., 2015; Ploeger and Birner, 2016; Young et al., 2018; Akritidis et al., 2019; Griffiths et al., 2020; Liao et al., 2021). Subsequent stratospheric intrusions can then lead to an increased stratosphere–troposphere exchange of O_3 as a result of this enrichment, particularly in spring when the lowermost stratospheric reservoir of O_3 reaches its annual maximum and is seasonally "flushed" thereafter (Hegglin and Shepherd, 2007; Bönisch et al., 2009). However, this process depends on changes in the BDC's deep and shallow branches. Strengthening of the deep branch increases to lowermost stratospheric O_3, while strengthening of the shallow branch favors enhanced transport and mixing of low-O_3 air from the tropical upper troposphere (Plumb, 2002; Bönisch et al., 2009). A study using a coupled atmosphere–ocean model with interactive stratospheric chemistry projects a 20 %–30 % increase in global stratosphere-to-troposphere transport (STT) O_3 flux from 1965 to 2095, as a result of an accelerated stratospheric BDC under an intermediate climate change scenario (Hegglin and Shepherd, 2009). Furthermore, chemistry–climate models (CCMs) predict an even larger increase in the STT O_3 flux (25 %–80 %) under climate change scenarios such as Representative Concentration Pathway (RCP) 8.5 (Collins, 2003; Sudo et al., 2003; Meul et al., 2018). Notably, Williams et al. (2019) identified an enhanced STT of O_3 over Asia and the Pacific region during 1980–2010 based on two different CCMs. The shallow branch of the BDC is associated with the breaking of synoptic and planetary-scale waves in the subtropical lower stratosphere (Plumb, 2002; Birner and Bönisch, 2011). Several multi-scale processes in proximity to the tropopause lead to irreversible STT events, including Rossby-wave breaking, tropospheric cyclones, cutoff lows, and tropopause-folding events (Holton et al., 1995). On a regional basis, including East Asia and its coastal area, subtropical westerly jets modulate the location, timing, and frequency of tropopause folds (Sprenger et al., 2003; Albers et al., 2018). Satellite measurements of O_3 and water vapor over 6 years were used to quantify the impact of a changing stratospheric circulation on tropospheric O_3 in the Northern Hemisphere (Neu et al., 2014). These observation-based results support the modeling studies showing that the intensified stratospheric BDC tends to enhance the impact of the stratospheric intrusions on tropospheric O_3. However, the conclusions drawn from the numerical studies have not yet been validated through long-term O_3 measurements, particularly O_3 sounding data (Trickl et al., 2011).

From 1990 onward, a significant amount of the anthropogenic emissions responsible for O_3 formation have shifted from North America and Europe to Asia (Granier et al., 2011; Cooper et al., 2014; Zhang et al., 2016). In East Asia, the overall long-term trend of the daytime average near-surface O_3 is 0.45 ppb a^{-1}, contrasting with a trend of -0.28 ppb a^{-1} in North America in the summertime (April–September) during 2000–2014 (Chang et al., 2017). Several studies have documented the increase in emissions of O_3 precursors at a few sites available for evaluating the long-term trends across East Asia (Ma et al., 2016; Sun et al., 2016; Xu et al., 2016; Wang et al., 2017). On the other hand, some regions in East Asia have seen a decline in precursor emissions after 2004, such as Beijing, Hong Kong, and Japan, due to local emission control efforts (Krotkov et al., 2016; Liu et al., 2016; Miyazaki et al., 2017; van der A et al., 2017). Elevated NO_2 emissions over megacities in China were possibly transported to Japan, potentially offsetting the local emission control efforts (Duncan et al., 2016). Further research is required to understand the long-term changes in tropospheric O_3, especially in East Asia, where rapid economic growth coincides with strict environmental regulations.

In this study, we present 30 years of O_3 observations from balloon soundings with a focus on latitudinal differences. To this end, observations from four sounding sites are analyzed together with model simulation results to quantify the long-term trends of middle-to-upper tropospheric O_3 and contributions of different origins along the northwestern Pacific coastal region. We are particularly interested in the regional difference near 30° N, the transition zone between the Hadley and Ferrel circulation cells, where the subtropical jet (STJ) prevails and where tropopause folding is frequently observed (Škerlak et al., 2015; Zhao et al., 2021). The specific questions to be addressed by this study are the following. (1) How do O_3 trends in the middle-to-upper troposphere vary with

latitude and season over the northwestern Pacific coastal regions, and are these observed trends consistent with those derived from a chemistry–climate model? (2) To what extent are these tropospheric O_3 changes linked to stratospheric influences? And (3) to what extent are these tropospheric O_3 changes linked to tropospheric sources, i.e., photochemical O_3 production due to biogenic and anthropogenic precursor emissions? The study aims to provide observational evidence to validate and constrain the CCMs' predictions of climate change impact on tropospheric O_3 in East Asia (e.g., Williams et al., 2019) where such information is still lacking.

2 Data and method

2.1 Ozonesonde observations

Around 30 years of O_3 sounding data at four sites along the northwestern Pacific coastal regions (Sapporo, Tsukuba, Naha, and Hong Kong) are used to characterize spatiotemporal variations of O_3 in the troposphere. Ozonesondes are launched around 14:00 LST (local standard time) once a week, which corresponds to the time when photochemical production reaches its daily maximum (Oltmans et al., 2004). The ozonesonde measurements include O_3 partial pressure, temperature, relative humidity, wind speed, and wind direction. Vertical O_3 measurements range from the surface to the middle stratosphere, approaching 30 km. The Hong Kong site has continually operated the electrochemical concentration cell (ECC) instrument since the beginning of its record. For the three sites in Japan, the O_3 sounding data were measured by carbon–iodine (CI) ozonesondes with 10 s recording intervals before 2009 and were changed to the ECC instrument with 2 s recording intervals after 2009. The operating principle of both CI ozonesondes and ECC ozonesondes is based on the reaction of O_3 to potassium iodide solution, wherein free iodine is liberated (Johnson et al., 2002; Witte et al., 2018). However, the transition of the measurement technology from CI to ECC around 2009 led to uncertainties and an overestimation of the long-term O_3 trends due to a step change in the resulting time series (Fig. S1 in the Supplement). Cross-evaluation of Ozone Monitoring Instrument (OMI) data and the ozonesonde observations at the Japan sites indeed showed that CI ozonesonde measurements of tropospheric O_3 columns are negatively biased relative to ECC measurements by 2–4 DU (Dobson unit) compared with the OMI data (Bak et al., 2019). A correction factor was applied to the O_3 profiles during the CI measurement period to remedy the problem. However, the applied factors were found to inaccurately impact observed tropospheric O_3 values (Morris et al., 2013). Removing the correction factor in the CI measurements can improve the consistency of ozonesondes with OMI data (Morris et al., 2013). We thus removed the correction factor applied to the original ozonesonde data available from the WOUDC for these three Japanese sounding stations hereinafter. After remov-

ing the correction factors for the observation period, the corrected datasets show no notable step changes around 2009 at the Japanese sites anymore (Fig. S2). It is worth noting that the conclusion we draw from current available long-term ozonesonde observations has limitations on the long-term trends but still has important implications for the understanding of tropospheric O_3 changes and model evaluations. The weekly launch frequency of the ozonesondes has been validated as reliable in representing long-term O_3 trends, as evidenced by comparing data with near-surface O_3 trends at an hourly time resolution (Liao et al., 2021). Summaries of ozonesonde site location and data availability are presented in Table 1 and Fig. 1.
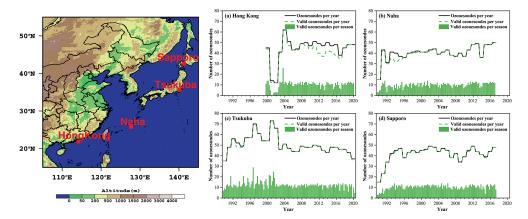
We limit our analyses of tropospheric and lower-stratospheric O_3 profiles to altitudes below 18 km, and we removed duplicate O_3 values during the descent period at the same heights in the time series to prevent redundant measurements as well as to reduce the uncertainty of solution evaporation and loss due to the O_3 sounding balloon bursting and/or tumbling through the atmosphere. O_3 profiles with continuous data missing more than a 200 m vertical coverage were excluded. The selected valid O_3 profiles with 10 or 2 s recording intervals were linearly interpolated to 10 m vertical intervals and then averaged to 50 m data points. The O_3 profiles after the quality control with 50 m vertical resolution were used for further analysis.

Due to the latitudinal differences and the seasonal variations in tropopause height across the four O_3 sounding observation sites, it is inappropriate to apply a specific height as the tropopause height. We thus employ the World Meteorological Organization lapse rate tropopause definition to calculate the tropopause height (hereafter called Z_t) for each site and O_3 profile. Z_t is defined as the level at which the lapse rate decreases to $2\,K\,km^{-1}$ or less, provided that the average lapse rate between this level and all higher levels within 2 km does not exceed $2\,K\,km^{-1}$ (WMO, 1957).

To better compare O_3 levels and trends at different latitudes within the troposphere, we normalize the height of each O_3 profile between 0 and 1 by dividing the altitude by the tropopause height Z_t. The upper troposphere (UT) is then defined by the normalized height (Z/Z_t) range between 0.7 and 0.9. The middle troposphere (MT) and lower troposphere (LT) are 0.4–0.6 and 0–0.2 Z/Z_t, respectively.

2.2 EMAC model and simulation setup

In this study, the European Centre for Medium-Range Weather Forecasts (ECMWF) Hamburg (ECHAM)/Modular Earth Submodel System (MESSy) Atmospheric Chemistry (EMAC) model is utilized to investigate the long-term changes in tropospheric O_3 and to quantify the relative contributions of different driving factors. The EMAC model is a global model that considers the interaction of chemistry and dynamic processes between the surface and the middle atmosphere (Jöckel et al., 2016). The reference simulation with

Figure 1. Locations of O_3 sounding sites (left panel), seasonal and annual ozonesonde sampling numbers (right panels) at **(a)** Hong Kong, **(b)** Naha, **(c)** Tsukuba, and **(d)** Sapporo. The continuous line shows the number of ozonesondes launched per year. The bars show the corresponding number per season. The dashed line indicates the number of valid ozonesondes per year, reaching up to 18 km altitude. Publisher's remark: please note that the above figure contains disputed territories. Publisher's remark: please note that the above figure contains disputed territories.

Table 1. Locations of O_3 sounding sites, measurement periods, and total data available along the northwestern Pacific coastal region.

Station	Latitude	Longitude	Ele-vation (m)	Period	Total data	Valid data (18 km)
Sapporo	43.10° N	141.30° E	19	1990–2017	1167	1159 (99 %)
Tsukuba	36.06° N	140.13° E	31	1990–2020	1564	1556 (99 %)
Naha	26.20° N	127.70° E	27	1990–2017	1137	1114 (98 %)
Hong Kong	22.31° N	114.17° E	66	2000–2020	929	863 (93 %)

specific dynamics (REF-D1) results from the EMAC model is used in this study (Jöckel et al., 2024a, b). The REF-D1 experiment is a hindcast simulation of the atmospheric state, using a prescribed sea surface temperature and sea ice from observations along with forcing for the extra-terrestrial solar flux, long-lived greenhouse gases, O_3-depleting substances, stratospheric aerosols, and an imposed Quasi-Biennial Oscillation that approximates the observed variations over the historical period to the fullest extent possible. The hindcast simulations are performed from 1980 to 2019 with the specific dynamics nudging by Newtonian relaxation toward ECMWF ERA-5 reanalysis meteorological data (Hersbach et al., 2020), including temperature, logarithm of surface pressure, divergence, and vorticity.

The simulations are conducted at a T42 (triangular) spectral resolution corresponding to an approximately $2.8° \times 2.8°$ quadratic Gaussian grid, 90 hybrid sigma-pressure vertical levels from surface up to 0.01 hPa and a 720 s time step (Jöckel et al., 2016). EMAC uses chemical submodels, the Module Efficiently Calculating the Chemistry of Atmosphere (MECCA; Sander et al., 2011) and the scavenging submodel (SCAV; Tost et al., 2006), to describe comprehensive chemical reaction mechanisms in gas and liquid phases that include O_3, CH_4, HO_x, and NO_x chemistry; non-methane hydrocar-

bon (NMHC) chemistry up to C_4; and isoprene, halogen (Cl and Br), and sulfur chemistry.

Emissions of lightning NO_x and soil NO_x are calculated using the submodels LNOX (Tost et al., 2007) and online emissions (ONEMIS) (Kerkweg et al., 2006; Jöckel et al., 2016), respectively. EMAC simulates the photolysis (using submodel JVAL; Sander et al., 2014) and shortwave radiation schemes (FUBRAD; Kunze et al., 2014) consistently, with particular regard for the evolution of the 11-year solar cycle (Morgenstern et al., 2017). For anthropogenic emissions, mixing ratios of greenhouse gases, O_3-depleting substances (ODSs), and other boundary conditions, the EMAC model setup follows the Chemistry-Climate Model Initiative (CCMI) 2020 protocol of the refD1 hindcast simulations (SPARC, 2010).

The EMAC model provides the diagnostic tracer O_3S (meaning O_3 of stratospheric origin) to directly measure the stratosphere-to-troposphere exchange of O_3. The O_3S tracer is transported across the tropopause into the troposphere and is removed by tropospheric O_3 reactions (Jöckel et al., 2006, 2016). When O_3S re-enters the stratosphere, it is re-initialized (Roelofs and Lelieveld, 1997). The tropospheric O_3 source (O_3T) is here calculated as tropospheric O_3 minus stratospheric O_3 ($O_3T = O_3 - O_3S$).

To better compare the model results with the observations, the simulation data were extracted from the grid boxes nearest to the observation sites. Specifically, 200 hPa was chosen for Hong Kong and Naha and 400 hPa was chosen for Tsukuba and Sapporo to represent the upper troposphere. The middle troposphere is defined at 500 hPa, while the lower troposphere is represented by 850 hPa in the model results. To assess the statistical significance of the differences, a paired two-sided t test ($p < 0.05$) was conducted for comparison.
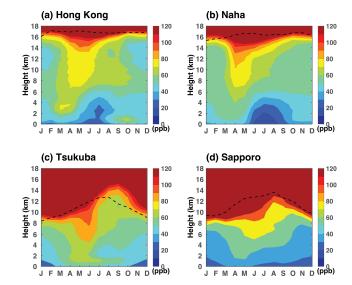
3 Results

3.1 Observational changes at different stations

3.1.1 Climatological distribution of tropospheric O_3

Figure 2 depicts the monthly climatological vertically resolved tropospheric O_3 distribution throughout the year. The four sites all show a distinct tongue-shaped pattern in the top-down direction characterized by high concentrations of O_3 greater than 70 ppb, each exhibiting peak levels in distinct months. The O_3 tongue extends from the lower stratosphere to the middle troposphere, even further spreading downward to the lower troposphere. In subtropical regions such as Hong Kong and Naha, the O_3 tongue starts to appear in early spring. The timing of appearance becomes progressively delayed when moving toward higher latitudes, with peak occurrences observed in Tsukuba during June and Sapporo in July (Fig. 2c–d). For the midlatitudes over the Pacific region, the incidence of stratospheric intrusions has been found to have a strong correlation with the location of the STJ (Zhao et al., 2021). The northward shift of the STJ with seasons agrees well with the occurrence of the O_3 tongues in different months over the four sites along the northwest Pacific coastal regions (Fig. S3). Tropopause-folding events are located preferentially on the southern flank of the STJ, with the associated stratosphere-to-troposphere transport of O_3 thus potentially contributing to the observed seasonal lag in the occurrence of the O_3 tongues (Fig. S4).

On the other hand, the four sites display distinct month–height cross-section distribution patterns of O_3. In near-tropical regions such as Hong Kong and Naha during the summer, a relatively clean layer with O_3 mixing ratios of less than 40 ppbv extends from the surface to about 5.0 km above the ground level. Such a structure, characterized by low concentrations in the lower troposphere, is not observed at the other two high-latitude sites. The unfavorable meteorological conditions linked to the East Asian monsoon such as a strong wind, precipitation, and less radiation could lead to significant O_3 scavenging and less photochemical production. This suggests that the East Asian summer monsoon has a more significant impact on O_3 vertical structures at lower latitude sites compared to high-latitude sites (Zhou et al., 2013). Meanwhile, it is noticed that high O_3 mixing ratios
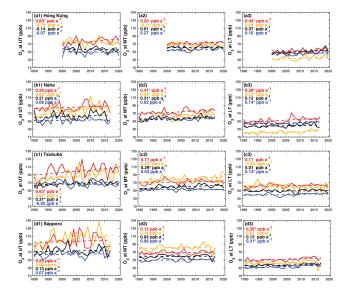

Figure 2. Month–height cross-sections of monthly mean O_3 at four O_3 sounding sites: **(a)** Hong Kong, **(b)** Naha, **(c)** Tsukuba, and **(d)** Sapporo (2000 to 2020 for Hong Kong, 1990 to 2017 for Naha and Sapporo, 1990–2020 for Tsukuba), from 1990 to 2017/2020 (2000 to 2020 for Hong Kong). Dashed black lines indicate the multiyear average tropopause height calculated by observations according to the World Meteorological Organization (WMO) lapse rate tropopause definition.

appear within the atmospheric boundary layer (ABL) (0.7–1.6 km according to Su et al., 2017) in Hong Kong in autumn (Fig. 2a), which represents the combined effect of local emissions and regional transport. During this season, the prevailing winds are predominantly from northwest to north, which could bring elevated levels of O_3 and its precursors from the Pearl River Delta region, a major manufacturing base in China, to Hong Kong (Ding et al., 2013; Lin et al., 2021).

3.1.2 Long-term trends in different layers of the troposphere

Figure 3 presents the long-term trends of O_3 in the upper, middle, and lower troposphere. In general, O_3 in the upper troposphere shows larger increases during boreal spring and summer than autumn and winter among the four sites except for Hong Kong. The largest O_3 trends are observed at Naha with an increase of 0.82 ppb a^{-1} during the summer and at Tsukuba (0.63 ppb a^{-1}) during the spring (at a 95 % confidence level). Hong Kong only shows a significant O_3 increase in spring with 0.60 ppb a^{-1}, while Tsukuba exhibits an extensive O_3 increase except in winter. For the Sapporo site, substantial positive O_3 changes are observed during summer but not statistically significant due to large temporal variabilities. This finding implies the importance of the STJ in the change of O_3 in the upper troposphere at Naha and Tsukuba. The locations are situated within the transitional zone between the Hadley and Ferrel circulation cells

Figure 3. Long-term changes in O_3 in the upper troposphere (UT, defined as 0.7–0.9 tropopause normalized height, first column), middle troposphere (MT, defined as 0.4–0.6 tropopause normalized height, second column), and lower troposphere (LT, defined as 0–0.2 tropopause normalized height, third column) in boreal spring (MAM, red lines), summer (JJA, yellow lines), autumn (SON, black lines), and winter (DJF, blue lines) at Hong Kong **(a1–a3)**, Naha **(b1–b3)**, Tsukuba **(c1–c3)**, and Sapporo **(d1–d3)**. Trends with a star symbol (*) indicate significance at the 95 % confidence level.

in spring and summer, as illustrated in Fig. S3. This influence appears more pronounced in comparison to the other two sites, namely, Hong Kong and Sapporo, which are situated further from this transitional zone.

Moving to the middle troposphere, Naha and Tsukuba consistently display an O_3 increase during all four seasons. The changes at these two sites in spring, summer, and autumn are more evident than those at the other two sites or in winter. This suggests a potential strengthened contribution from regional transport and stratospheric intrusion for these two sites. In addition, lightning-produced NO_x emissions contribute to major events of O_3 in the middle-to-upper troposphere over convection-active regions (Liu et al., 2002; Zhang et al., 2012). How those factors contribute to O_3 enhancement remains a question for further investigations.

In the lower troposphere, substantial O_3 increases are observed at all sites in spring except Tsukuba. O_3 enhancement in the lower troposphere over Hong Kong during springtime is associated with either equatorial Northern Hemisphere biomass burning in Africa or Southeast Asian biomass burning (Oltmans et al., 2004). The Tsukuba site experienced a slight decrease in summer over the past 3 decades. Such a decrease could be primarily attributed to the changes in anthropogenic emissions in East Asia (Li et al., 2019).
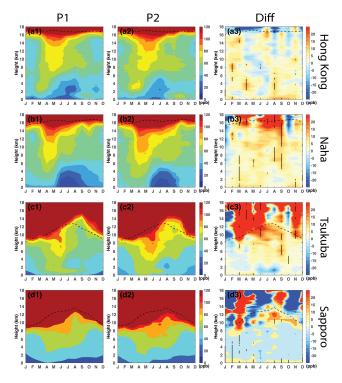
Overall, the long-term changes in tropospheric O_3 display considerable variability, contingent on the atmospheric layers (i.e., low, middle, and upper) and the geographical latitude

of observation sites. Naha, Tsukuba, and Sapporo exhibited an increase in the middle-to-upper troposphere. A substantial rise is observed in the upper troposphere during summer over Naha (0.82 ppb a^{-1}) and spring over Tsukuba (0.63 ppb a^{-1}). When compared to the other three sites, changes in the middle-to-upper troposphere over Hong Kong are smaller or negative, except during springtime. All four sites demonstrated an increase in O_3 mixing ratios across the four seasons in the lower troposphere, except for summer in Tsukuba. Investigating the driving factors behind such differences in change becomes one of the objectives of this study. A more comprehensive exploration of O_3 origin and its contributions to the changes in tropospheric O_3 will be discussed in Sect. 3.2, leveraging modeling results to provide deeper insights.

3.1.3 Changes in composite O_3 cross-sections between decades

Tropospheric O_3 shows a larger variability in the upper troposphere compared to the middle and lower troposphere (Fig. 3a1–d3). Such a large variability, likely driven by transport and dynamics in the tropopause region, impedes drawing definite conclusions on long-term trends for single measurement sites with infrequent sampling. Therefore, the aggregation of tropospheric O_3 during the early and late decades is expected to provide more robust insights.

Figure 4 illustrates the vertically resolved tropospheric O_3 distributions and changes between the early (the 1990s for Naha, Tsukuba, and Sapporo; the 2000s for Hong Kong) and late (the 2010s) decades as a function of the month. Their respective tropospheric O_3 changes over the same period (i.e., the 2000s to 2010s) at the four sites are presented in Figure S5 to demonstrate the consistency of the results. The time lag pattern for the O_3 tongue remains the same from April in the southern site of Hong Kong to July in the northern site of Sapporo for the first and the last decades (Fig. 4a1–d1). However, there are noticeable increases in O_3 mixing ratios and a deeper layer extension of the O_3 concentration greater than 80 ppbv from the stratosphere to the troposphere at Naha and Tsukuba over the past several decades (Fig. 4a2–d2).
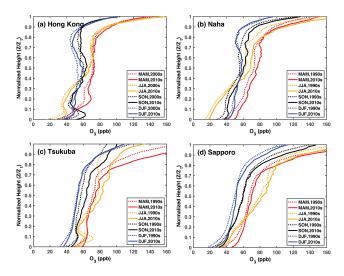
As illustrated in Fig. 4a3–d3, Naha, Tsukuba, and Sapporo exhibit significant enhancements of O_3 from the middle-to-upper troposphere to the lowermost stratosphere. In contrast to the three sites in Japan, Hong Kong shows more significant O_3 changes in the lower troposphere. The buildup of lowermost stratospheric (LMS) O_3 happens from winter to spring, thus the STT flux of O_3 normally reaches its peak during late spring to early summer in the extratropical regions (e.g., Škerlak et al., 2015; Albers et al., 2018). The O_3 tongue during the spring and summer is possibly associated with enhanced contributions from stratospheric intrusions. While it may be tempting to conclude that such an O_3 increase primarily originates from the stratosphere due to its proximity, observational data alone cannot provide a definite

Figure 4. Month–height cross-sections of monthly mean composite O_3 in the first period P1 (the 1990s for Naha, Tsukuba, and Sapporo but the 2000s for Hong Kong), the last period (P2: 2010s), and the differences in O_3 between P2 and P1 at **(a1–a3)** Hong Kong, **(b1–b3)** Naha, **(c1–c3)** Tsukuba, and **(d1–d3)** Sapporo. Dashed black lines indicate the tropopause heights calculated by observations according to the WMO lapse rate tropopause definition. Dashed lines in the a3–d3 column represent the layer with statistically significant changes according to a paired two-sided t test ($p < 0.05$).

Figure 5. A comparison of vertical profiles of seasonal mean O_3 during spring (red), summer (yellow), autumn (black), and winter (blue) at four sites: **(a)** Hong Kong, **(b)** Naha, **(c)** Tsukuba, and **(d)** Sapporo between the first and the last decades.

conclusion. Additionally, different locations among the four sites may introduce further differences in O_3 sources.

Figures 5b-d present a comparison of seasonally averaged vertical O_3 profiles between the 1990s and the 2010s at the Naha, Tsukuba, and Sapporo sites. A parallel analysis is conducted for Hong Kong but for a comparison between the 2000s and 2010s (Fig. 5a). While the general trend indicates an increase in O_3 mixing ratios with altitude, with higher values during spring and summer, several noteworthy features are identified from Fig. 5. Firstly, vertical O_3 profiles vary with latitude and season. For instance, Hong Kong and Tsukuba show O_3 peaks within the ABL in autumn (black lines) and during summer (yellow lines), respectively. These peaks suggest a predominant influence of local anthropogenic emissions during the warmer months. A substantial O_3 peak at Hong Kong is observed around 0.2 normalized height (around 3–4 km above ground level) during spring. This enhancement is attributed to a combination of stratospheric intrusions and the transboundary transport of biomass-burning emissions originating from Southeast Asia (Liao et al., 2021; Zhao et al., 2021). On the other hand, Naha

and Sapporo do not exhibit discernible peaks in the lower troposphere, suggesting a relatively smaller impact from the combination of near-surface factors and stratospheric intrusions.

Secondly, the seasonal minimum O_3 mixing ratios in the lower troposphere are observed during summer rather than winter, contrasting with the middle-to-upper troposphere observations over Hong Kong and Naha. This seasonal difference in the lower troposphere could be attributed to the influence of the East Asian monsoon as discussed earlier. In the middle-to-upper troposphere, there are no such significant seasonal differences among sites. Conversely, the minimum seasonal O_3 mixing ratios occur during winter throughout the entire troposphere at the other two sites.

Thirdly, enhancements of O_3 in the middle and upper troposphere are considerably more pronounced over Naha, Tsukuba, and Sapporo than over Hong Kong during the warm seasons (spring and summer) over the past 3 decades. This enhancement is particularly significant in the upper troposphere in Naha and Tsukuba during summer, as indicated by the dashed and solid yellow lines. In Hong Kong, enhancements are primarily observed at the top of the ABL in spring and within the ABL in autumn, corresponding to where seasonal maxima are observed. These findings align with previous research (Huang et al., 2005; Ding et al., 2013; Liao et al., 2021; Lin et al., 2021).

3.2 Comparison with observations and stratospheric vs. tropospheric attribution using EMAC simulations
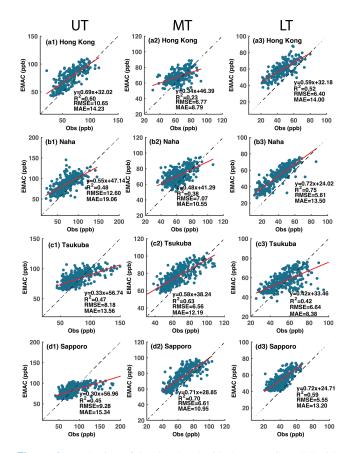
In order to substantiate the observational findings, we now turn to the quantification of the relative contributions of key

drivers to the observed changes in tropospheric O_3 based on the EMAC simulations.

3.2.1 Evaluation of EMAC simulations

The EMAC simulations of O_3 for different altitude ranges in the troposphere are further evaluated with the O_3 sounding data during the study period. As illustrated in Fig. 6, a majority of data points are located above the 1:1 line at all sites, indicating that EMAC overpredicts O_3 in the troposphere, which agrees with other related studies (Jöckel et al., 2016; Young et al., 2018; Revell et al., 2018). The root-mean-square error (RMSE) and mean absolute error (MAE) of O_3 are generally larger in the UT than in MT and LT. The EMAC model shows a better representation in the upper and lower troposphere than in the middle troposphere in Hong Kong and Naha, as indicated by the coefficient of determinations (R^2). For instance, R^2 reaches the highest value of 0.75 in the lower troposphere over Naha (Fig. 6b3), whereas R^2 is only about 0.23 for the middle troposphere over Hong Kong (Fig. 6a2). As for the midlatitude sites, Tsukuba and Sapporo, the EMAC model shows a relatively good representation of O_3 in the different layers of the troposphere, despite the overall overestimation, in contrast to the Hong Kong and Naha sites with highest R^2 in the MT. It is worth noting that although EMAC generally overestimates O_3, there is a tendency toward higher overestimation for lower O_3 mixing ratios and lower overestimation at higher O_3 mixing ratios, especially for the UT O_3 at the Tsukuba and Sapporo sites (Fig. 6c1, d1).

Furthermore, the EMAC model predicts the realistic long-term trends of O_3 at different levels of the troposphere as indicated by the similar O_3 changes between monthly mean observation and model (Fig. 7), as well as the comparable long-term change rates of model-predicted O_3 with the observations (Table 2). For example, the largest positive O_3 trends in the model also occur in the upper troposphere over Naha during summer at $0.75\ \mathrm{ppb\ a^{-1}}$, slightly less than the observations with $0.82\ \mathrm{ppb\ a^{-1}}$ for the past 3 decades (Table 2). Except for Hong Kong, the other three sites in the north have larger positive trends of O_3 in the upper troposphere than in the middle and lower troposphere from spring to autumn. Hong Kong shows a relatively large positive trend of O_3 in the middle and lower troposphere compared to other sites during the past 30 years.

Figure 8 demonstrates the month–height cross-sections of EMAC-predicted monthly mean O_3 and their changes in the troposphere at the four sites between the 1990s and 2010s. Compared with the observed counterparts (Fig. 4), the model reproduces the temporal and spatial variation patterns of tropospheric O_3 within the troposphere quantitatively well. Specifically, the model captures a key feature with the O_3 tongue that occurs from late spring to early summer over four sites and their variation with latitude. The summer relatively clean layer with low O_3 mixing ratios in the lower tropo-

Figure 6. Evaluation of O_3 simulated with the EMAC model with observations in the upper troposphere (UT), middle troposphere (MT), and lower troposphere (LT) at the four sites: **(a1–a3)** Hong Kong, **(b1–b3)** Naha, **(c1–c3)** Tsukuba, and **(d1–d3)** Sapporo. The red lines are linear regression results between the observations and the EMAC model results. Dashed black lines represent the 1:1 line for reference. The statistical metrics including the coefficient of determination (R^2), root mean standard error (RMSE), and mean absolute error (MAE) are included for the quantitative evaluation of the model performance.

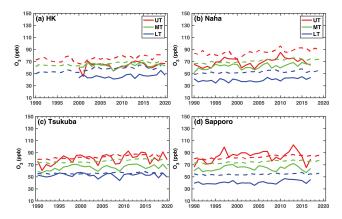sphere at the southern sites of Hong Kong and Naha is also well simulated.

Overall, the EMAC model reasonably simulates the spatial and temporal variations in tropospheric O_3 as compared to the O_3 observations at the four sounding sites. Consistency between the model and observations suggests that the trends observed in the Japanese ozonesondes remain valuable despite uncertainties related to the transitions between the two types of ozonesondes. Moreover, the model can effectively be used to investigate the drivers of these trends.

3.2.2 Changes in O_3S and O_3T derived from EMAC simulations

To gain deeper insights into the factors contributing to tropospheric O_3, we analyze the EMAC-simulated total O_3 in the troposphere, the origin of O_3 from the stratosphere

Table 2. The trends of EMAC-simulated O_3 (ppb a^{-1}) in the upper, middle, and lower troposphere in different seasons from 1990 to 2019. The observational O_3 trends are indicated in parentheses for comparison with the three Japanese sites. For the Hong Kong site, the O_3 trends since 2000 for both model (the first value) and observations (the second value) are in square brackets. Note that observational periods for the three Japanese sites are slightly different from the model (See Table 1). The trends with star symbols (*) indicate the 95 % confidence level. Bold indicates agreement with the observations for significance and the sign of the trend. The trends with the same sign and both not significant are also indicated by bold. Normal font indicates agreement with the sign of the trend but not for significance, and italics indicate agreement with the opposite sign of the trend.

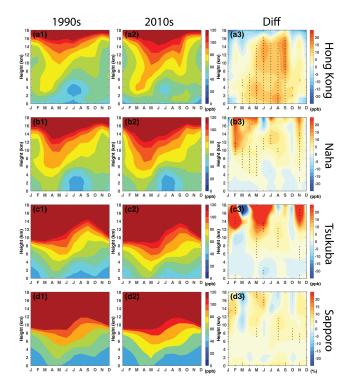| Station		MAM	JJA	SON	DJF
Hong Kong	UT	**0.49* [0.98*	0.60*]**	0.56* [*0.49**	−0.15]	0.32* [*0.34*	−0.14]	0.06 [*0.25*	−0.07]
	MT	0.33* [0.65*	0.20]	0.43* [*0.39**	−0.11]	0.36* [0.29	0.01]	0.01 [−*0.01*	0.27]
	LT	**0.49* [0.65*	0.44*]**	0.56* [0.53*	0.26]	**0.32* [0.16	0.37]**	0.06 [−*0.18*	0.16]
Naha	UT	0.33* (0.26)	**0.75* (0.82*)**	0.37* (0.21)	**0.05 (0.06)**
	MT	**0.42* (0.41*)**	**0.33* (0.44*)**	**0.33* (0.31*)**	0.10* (0.02)
	LT	**0.32* (0.38*)**	**0.21* (0.23*)**	**0.09 (0.13)**	**0.08* (0.14*)**
Tsukuba	UT	**0.26* (0.63*)**	**0.45* (0.67*)**	**0.32* (0.31*)**	*0.12 (−0.05)*
	MT	0.21* (0.17)	**0.37* (0.42*)**	**0.28* (0.29*)**	0.14* (0.03)
	LT	0.13* (0.11)	*0.09 (−0.20)*	0.03 (0.01)	**0.05* (0.13*)**
Sapporo	UT	0.22* (0.26)	0.34* (0.68)	0.25* (0.13)	0.15* (0.07)
	MT	0.18* (0.12)	0.28* (0.14)	0.21* (0.04)	0.11* (0.06)
	LT	**0.12* (0.29*)**	0.12* (0.05)	**0.03 (0.13)**	0.03 (0.31*)

Figure 7. Time series of monthly mean O_3 for ozonesonde measurements (solid lines) and the EMAC model (dashed lines) for four sites **(a)** Hong Kong (HK), **(b)** Naha, **(c)** Tsukuba, and **(d)** Sapporo at different layers of the troposphere.

(i.e., stratospheric intrusion, O_3S), and the origin of O_3 from the troposphere (i.e., photochemical production in the troposphere, O_3T) at the four sites, along with their latitudinal variations (Figs. 9 and 10). The layer with the high mixing ratio of O_3S extending from the lower stratosphere to the troposphere occurs in early spring at the southern site (i.e., Hong Kong). Conversely, similar occurrences are observed to shift to early summer in the northern site (i.e., Sapporo) (Fig. 9). The seasonal buildup of midlatitude total O_3 typically unfolds from winter through to late spring, followed by a decline in summer (Fioletov and Shepherd, 2003). The seasonal lifting of the tropopause will naturally contribute to

the entrainment of O_3-rich air from the stratosphere into the troposphere (Monks, 2000). Furthermore, together with dynamical processes such as tropopause folding in the vicinity of the subtropical jet (Baray et al., 2000), stratospheric O_3 is transported downward into the troposphere. Over the past 30 years, the two sites within the subtropics (Tsukuba at 36° N and Sapporo at 43° N) have exhibited larger O_3S increases in the lower stratosphere and upper troposphere compared to the other two sites situated in the near-tropical region (Hong Kong at 22° N and Naha at 26° N).

The O_3T data show seasonal maxima during the warm seasons (from March to October) throughout the troposphere in Hong Kong, while mainly occurring in the middle-to-upper troposphere among the three Japanese sites (Fig. 10). In the lower troposphere at Hong Kong, the O_3T contributes more than O_3S (60–80 ppb vs. 10–20 ppb) in the separated O_3 hotspots around 2–4 km during spring. In the tropical regions, air rises in the Hadley cell from the surface to the upper troposphere and further ascends into the stratosphere where it is transported to the midlatitudes by the BDC (Brewer, 1949; Stohl et al., 2003). In this way, the tropospheric-origin O_3 could be further transported to the middle-to-upper troposphere of midlatitude regions.

Several factors influence O_3 mixing ratios over the study regions, which could potentially be responsible for the local maxima in O_3T: transport from near-surface tropospheric O_3 within the upward branch of the Hadley cell into the upper troposphere; horizontal transport from upstream polluted regions, e.g., mainland China in this study; biomass-burning-related transport; enhanced mixture by active convection and lighting events; and local photochemical O_3 production. O_3T
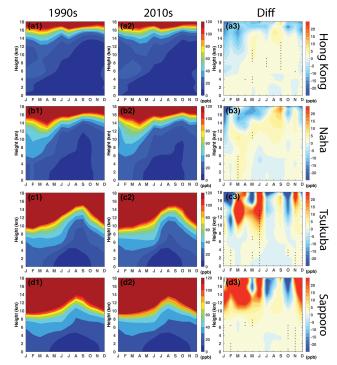
Figure 8. EMAC-simulated monthly mean O_3 in the 1990s and 2010s and their differences between 2010s and 1990s at the four observation sites of **(a1–a3)** Hong Kong, **(b1–b3)** Naha, **(c1–c3)** Tsukuba. and **(d1–d3)** Sapporo. The horizontal axes denote the months of the year, and the vertical axes represent the height above ground. Dots in panels **(a3)**–**(d3)** represent the layer with statistically significant changes according to a paired two-sided t test ($p < 0.05$).

Figure 9. A comparison of the EMAC-simulated monthly mean temporal and spatial distributions of O_3S in the 1990s and 2010s and the differences between the 2010s and 1990s at the four observation sites: **(a1–a3)** Hong Kong, **(b1–b3)** Naha, **(c1–c3)** Tsukuba, and **(d1–d3)** Sapporo. Dots represent the layer with statistically significant changes according to a paired two-sided t test ($p < 0.05$).

has shown significant enhancements among the four sites over the past several decades. However, the primary contributors to the high O_3T concentrations and their enhancement vary with locations and layers, which require further investigation.

3.2.3 Attribution of EMAC tropospheric O_3 changes: O_3S vs. O_3T

Utilizing the reasonably realistic simulations of tropospheric O_3 and their variations by the EMAC model, we can now quantify the respective contributions of O_3S and O_3T to the changes in tropospheric O_3 between the 2010s and 1990s, as presented in Table 3. Overall, the increase in O_3T (up to 11.09 ppb) dominates the O_3 increase throughout the troposphere at all sites during summer. Particularly for the near-tropical sites, Hong Kong and Naha, the increase in O_3T contributes more than the O_3S changes with percentage contributions greatly more than 60 %, even offsetting the decrease in O_3S during winter and spring. Conversely, for the subtropical sites Tsukuba and Sapporo, O_3S emerges as the primary driver for changes in the middle-to-upper tropospheric

O_3 during winter and spring. The contribution of O_3S to observed O_3 increases by up to 96 % at Sapporo in DJF and 40 % at Tsukuba in JJA in the upper troposphere (Table 3).
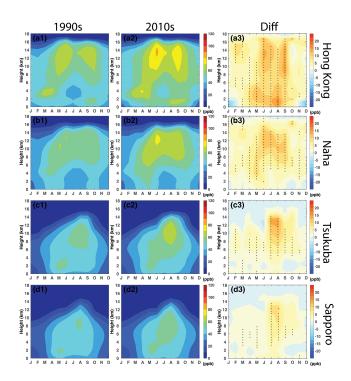
To get a more complete picture of how tropospheric O_3 changes along the northwest Pacific regions, the zonal mean of tropospheric O_3, O_3S, and O_3T changes are compared in Figs. 11 and S6. The climatological distribution of vertical tropospheric O_3 with latitude is determined by O_3S in the subtropics and O_3T in the tropics.

Tropospheric O_3 shows statistically significant positive changes from 10 to 60° N in summer, with the maximum in the middle-to-upper troposphere around 30° N. Similarly, O_3T demonstrates a similar pattern of changes as tropospheric O_3 in summer, indicating that tropospheric photochemical O_3 production is the primary driver of the summertime tropospheric O_3 enhancement. Strengthened downward transport of stratospheric O_3 primarily affects the upper troposphere in the subtropics during summer.

Conversely, during winter and spring, O_3S significantly contributes to the enhancement of tropospheric O_3 in the subtropics. Positive changes in O_3T are observed south of 40° N, partly offsetting the decrease in O_3S in the upper troposphere.

Table 3. Tropospheric O_3 changes and contributions from O_3S and O_3T to changes in tropospheric O_3 between the 2010s and 1990s at the upper, middle, and lower troposphere (UT, MT, and LT) in different seasons. The percentage contributions of O_3S and O_3T to O_3 changes are listed in the parentheses.

Station		O_3 changes (ppb)				O_3S changes (ppb)				O_3T changes (ppb)			
		MAM	JJA	SON	DJF	MAM	JJA	SON	DJF	MAM	JJA	SON	DJF
Hong Kong	UT	3.55	12.53	7.09	−0.40	−2.03 (−57 %)	1.44 (11 %)	1.41 (20 %)	−3.44 (860 %)	5.58 (157 %)	11.09 (89 %)	5.69 (80 %)	3.04 (−760 %)
	MT	6.35	9.22	7.50	0.32	1.30 (20 %)	0.96 (10 %)	1.23 (16 %)	−2.84 (−888 %)	5.06 (80 %)	8.27 (90 %)	6.27 (84 %)	3.16 (988 %)
	LT	9.62	11.47	6.28	2.10	0.88 (9 %)	0.10 (1 %)	−0.13 (−2 %)	1.24 (59 %)	8.73 (91 %)	11.37 (99 %)	6.41 (102 %)	0.86 (41 %)
Naha	UT	5.94	14.76	7.76	1.31	1.05 (18 %)	3.81 (26 %)	2.98 (38 %)	−1.87 (−143 %)	4.90 (82 %)	10.95 (74 %)	4.78 (62 %)	3.18 (243 %)
	MT	8.52	6.29	6.74	2.19	2.32 (27 %)	0.08 (1 %)	1.10 (16 %)	−1.03 (−47 %)	6.19 (73 %)	6.22 (99 %)	5.64 (84 %)	3.22 (147 %)
	LT	5.86	3.32	1.75	1.71	2.35 (40 %)	−0.19 (−6 %)	0.07 (4 %)	0.73 (43 %)	3.51 (60 %)	3.51 (106 %)	1.68 (96 %)	0.98 (57 %)
Tsukuba	UT	10.65	11.45	6.35	−2.08	7.33 (69 %)	4.23 (40 %)	2.19 (34 %)	−4.59 (221 %)	3.32 (31 %)	7.22 (60 %)	4.15 (66 %)	2.51 (−121 %)
	MT	4.54	7.39	5.18	2.74	1.50 (33 %)	2.10 (28 %)	1.39 (27 %)	0.51 (19 %)	3.04 (67 %)	5.29 (72 %)	3.79 (73 %)	2.23 (81 %)
	LT	2.50	2.17	0.24	0.98	1.27 (51 %)	0.44 (20 %)	0.94 (392 %)	0.90 (92 %)	1.22 (49 %)	1.74 (80 %)	−0.70 (−292 %)	0.08 (8 %)
Sapporo	UT	8.66	8.58	5.11	4.82	6.85 (79 %)	3.19 (37 %)	2.00 (39 %)	4.65 (96 %)	1.82 (21 %)	5.40 (63 %)	3.11 (61 %)	0.17 (4 %)
	MT	3.80	5.73	3.88	2.27	1.60 (42 %)	1.59 (28 %)	1.31 (34 %)	1.62 (71 %)	2.20 (58 %)	4.14 (72 %)	2.57 (66 %)	0.65 (29 %)
	LT	2.37	2.80	0.27	0.60	1.19 (50 %)	0.35 (13 %)	0.71 (263 %)	0.69 (115 %)	1.18 (50 %)	2.45 (87 %)	−0.45 (−163 %)	−0.09 (−15 %)

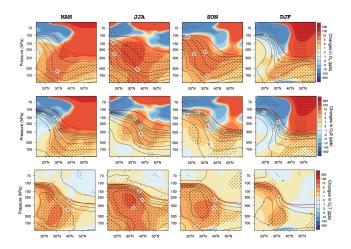

Figure 10. Similar to Fig. 9 but for the component of tropospheric O_3 (O_3T).

4 Discussion and conclusion

In this study, 30 years of ozonesonde observational data at four ozonesonde sites (Hong Kong, Naha, Tsukuba, and Sapporo) are presented together with simulation results of the chemistry–climate model EMAC to characterize the temporal and spatial variation patterns and the long-term changes in tropospheric O_3 along the northwest Pacific region.

The analysis of the seasonality in O_3 shows a seasonal maximum throughout the troposphere, occurring in late spring at the tropical site of Hong Kong and shifting to early summer at the midlatitude sites such as Sapporo. Additionally, for Hong Kong and Naha, the lower tropospheric O_3 exhibits a seasonal minimum. As for long-term changes, tropospheric O_3 generally increases at all four sites. Naha and Tsukuba show larger positive trends of O_3 up to 0.82 ppb a^{-1}, particularly in the upper and middle troposphere. The aggregation analysis between different decades indicates that the seasonal maximum in the troposphere becomes more pronounced and deeper over time.

Based on EMAC simulations, the summer and autumn enhancement of O_3 in the middle-to-upper troposphere is mostly attributable to a tropospheric O_3 source linked to increasing pollution emissions, with percentage contributions of more than 60 %. On the other hand, O_3 originating from the stratosphere accounts for the large portions of the middle-to-upper tropospheric O_3 enhancement, contributing 19 %–96 % during winter and 28 %–40 % during spring in the mid-

Figure 11. Latitude–pressure cross-sections of mixing ratio differences in O_3, O_3S, and O_3T (ppb) between the 2010s and 1990s along the northwest Pacific region (zonal mean over 110 to 150° E) in four seasons. Black lines indicate the climatological distribution. Solid red lines denote the tropopause height. Dots represent the layer with statistically significant changes according to a paired two-sided t test ($p < 0.05$).

latitudes. The climatological maximum observed in the seasonality of O_3 throughout the troposphere is associated with both stratosphere–troposphere exchange north of 30° N and photochemical O_3 production in the troposphere in spring. These findings corroborate the features discussed by Oltmans et al. (2004), confirming them with a longer observational dataset based on the tagged O_3 tracers in the EMAC model. Our results further confirm the offsetting effect of the O_3T increase on the decrease in O_3S in the tropical troposphere during winter and spring.

While the magnitude of O_3 trends is well simulated with the EMAC model in most atmospheric layers, uncertainties persist in the mean values due to various factors. These include large dynamical variability perturbing stratosphere-to-troposphere O_3 transport, the influence of O_3-depleting substances, uncertainties with long-term changes in emissions, insufficient treatment of chemical processes, or inaccurate transport due to excessive numerical diffusion in the tropopause region. Additionally, uncertainties may arise from interpolating the relatively coarse horizontal and vertical resolutions of the global model data to the locations of the observational sites. Nevertheless, the presented results indicate a satisfactory level of agreement between the model results and the observations, allowing further disentangling of O_3T vs. O_3S contributions.

The dynamical and chemical drivers for such long-term tropospheric changes deserve further analysis in the future. Here, we propose several mechanisms based on related research that could potentially contribute to observed tropospheric O_3 enhancements in East Asia. Regional transport is one important contributor to tropospheric O_3 enhancement.

Compared with the other two Japanese sites, Naha, to the east of China, is susceptible to regional transport of air pollution from China. The prevailing westerly winds bring O_3-enriched air from eastern China to Naha, resulting in a substantial increase in O_3 from the middle-to-upper troposphere. Internal dynamical variabilities such as the warm phase of the El Niño–Southern Oscillation (ENSO) and the easterly phase of the Quasi-Biennial Oscillation (QBO) are known to be closely tied to enhanced STT of O_3 (Neu et al., 2014; Zeng and Pyle, 2005). The ENSO/QBO-related changes can influence jet stream variations, leading to the formation of tropopause folds through Rossby-wave breaking (Albers et al., 2018). Increased frequency and the northward shift of tropopause-folding events are observed in the East Asia region (Fig. S7), attributed to an increase in the zonal wind and poleward–upward shift of the STJ driven by global warming-induced increases in greenhouse gases (Akritidis et al., 2019; Manney and Hegglin, 2018). With increasing greenhouse gases, the BDC tends to strengthen due to larger zonal-mean temperature gradients and increased wave drag in the extratropical stratosphere (Shepherd and McLandress, 2011; Neu et al., 2014). This results in an increased O_3 reservoir over the subtropical LMS, facilitating downward transport to the troposphere under the influence of the Pacific jet (Hegglin and Shepherd, 2009; Albers et al., 2018).

Review statement. This paper was edited by Pedro Jimenez-Guerrero and reviewed by four anonymous referees.

References

Akritidis, D., Pozzer, A., and Zanis, P.: On the impact of future climate change on tropopause folds and tropospheric ozone, Atmos. Chem. Phys., 19, 14387–14401, https://doi.org/10.5194/acp-19-14387-2019, 2019.

Albers, J. R., Perlwitz, J., Butler, A. H., Birner, T., Kiladis, G. N., Lawrence, Z. D., Manney, G. L., Langford, A. O., and Dias, J.: Mechanisms governing interannual variability of stratosphere-to-troposphere ozone transport, J. Geophys. Res., 123, 234–260, https://doi.org/10.1002/2017JD026890, 2018.

Bak, J., Baek, K.-H., Kim, J.-H., Liu, X., Kim, J., and Chance, K.: Cross-evaluation of GEMS tropospheric ozone retrieval performance using OMI data and the use of an ozonesonde dataset over East Asia for validation, Atmos. Meas. Tech., 12, 5201–5215, https://doi.org/10.5194/amt-12-5201-2019, 2019.

Baray, J.-L., Daniel, V., Ancellet, G., and Legras, B.: Planetary-scale tropopause folds in the southern subtropics, Geophys. Res. Lett., 27, 353–356, https://doi.org/10.1029/1999GL010788, 2000.

Birner, T. and Bönisch, H.: Residual circulation trajectories and transit times into the extratropical lowermost stratosphere, Atmos. Chem. Phys., 11, 817–827, https://doi.org/10.5194/acp-11-817-2011, 2011.

Bönisch, H., Engel, A., Curtius, J., Birner, Th., and Hoor, P.: Quantifying transport into the lowermost stratosphere using simultaneous in-situ measurements of SF_6 and CO_2, Atmos. Chem. Phys., 9, 5905–5919, https://doi.org/10.5194/acp-9-5905-2009, 2009.

Brewer, A. W.: Evidence for a world circulation provided by the measurements of helium and water vapour distribution in the stratosphere, Q. J. Roy. Meteor. Soc., 75, 351–363, https://doi.org/10.1002/qj.49707532603, 1949.

Chang, K.-L., Petropavlovskikh, I., Cooper, O. R., Schultz, M. G., and Wang, T.: Regional trend analysis of surface ozone observations from monitoring networks in eastern North America, Europe and East Asia, Elem. Sci. Anth., 5, 50, https://doi.org/10.1525/elementa.243, 2017.

Collins, J. W.: Effect of stratosphere-troposphere exchange on the future tropospheric ozone trend, J. Geophys. Res., 108, 8528, https://doi.org/10.1029/2002JD002617, 2003.

Cooper, O. R., Parrish, D. D., Ziemke, J., Balashov, N. V., Cupeiro, M., Galbally, I. E., Gilge, S., Horowitz, L., Jensen, N. R., Lamarque, J.-F., Naik, V., Oltmans, S. J., Schwab, J., Shindell, D. T., Thompson, A. M., Thouret, V., Wang, Y., and Zbinden, R. M.: Global distribution and trends of tropospheric ozone: An observation-based review, Elem. Sci. Anth., 2, 000029, https://doi.org/10.12952/journal.elementa.000029, 2014.

Ding, A. J. and Wang, T.: Influence of stratosphere-to-troposphere exchange on the seasonal cycle of surface ozone at Mount Waliguan in western China, Geophys. Res. Lett., 33, L03803, https://doi.org/10.1029/2005GL024760, 2006.

Ding, A. J., Wang, T., and Fu, C. B.: Transport characteristics and origins of carbon monoxide and ozone in Hong Kong, South China, J. Geophys. Res., 118, 9475–9488, https://doi.org/10.1002/jgrd.50714, 2013.

Duncan, B. N., Lamsal, L. N., Thompson, A. M., Yoshida, Y., Lu, Z., Streets, D. G., Hurwitz, M. M., and Pickering, K. E.: A space-based, high-resolution view of notable changes in urban NO_x pollution around the world (2005–2014), J. Geophys. Res., 121, 976–996, https://doi.org/10.1002/2015JD024121, 2016.

Fioletov, V. E. and Shepherd, T. G.: Seasonal persistence of mid-latitude total ozone anomalies, Geophys. Res. Lett., 30, 1417, https://doi.org/10.1029/2002GL016739, 2003.

Granier, C., Bessagnet, B., Bond, T., D'Angiola, A., Denier van der Gon, H., Frost, G. J., Heil, A., Kaiser, J. W., Kinne, S., Klimont, Z., Kloster, S., Lamarque, J.-F., Liousse, C., Masui, T., Meleux, F., Mieville, A., Ohara, T., Raut, J.-C., Riahi, K., Schultz, M. G., Smith, S. J., Thompson, A., van Aardenne, J., van der Werf, G. R., and van Vuuren, D. P.: Evolution of anthropogenic and biomass burning emissions of air pollutants at global and regional scales during the 1980–2010 period, Clim. Change., 109, 163, https://doi.org/10.1007/s10584-011-0154-1, 2011.

Griffiths, P. T., Keeble, J., Shin, Y. M., Abraham, N. L., Archibald, A. T., and Pyle, J. A.: On the Changing Role of the Stratosphere on the Tropospheric Ozone Budget: 1979–2010, Geophys. Res. Lett., 47, e2019GL086901, https://doi.org/10.1029/2019GL086901, 2020.

Hegglin, M. I. and Shepherd, T. G.: O_3-N_2O correlations from the Atmospheric Chemistry Experiment: Revisiting a diagnostic of transport and chemistry in the stratosphere, J. Geophys. Res.-Atmos., 112, D19301, https://doi.org/10.1029/2006JD008281, 2007.

Hegglin, M. I. and Shepherd, T. G.: Large climate-induced changes in ultraviolet index and stratosphere-to-troposphere ozone flux, Nat. Geosci., 2, 687–691, https://doi.org/10.1038/ngeo604, 2009.

Hersbach, H., Bell, B., Berrisford, P., Hirahara, S., Horányi, A., Muñoz-Sabater, J., Nicolas, J., Peubey, C., Radu, R., Schepers, D., Simmons, A., Soci, C., Abdalla, S., Abellan, X., Balsamo, G., Bechtold, P., Biavati, G., Bidlot, J., Bonavita, M., De Chiara, G., Dahlgren, P., Dee, D., Diamantakis, M., Dragani, R., Flemming, J., Forbes, R., Fuentes, M., Geer, A., Haimberger, L., Healy, S., Hogan, R. J., Hólm, E., Janisková, M., Keeley, S., Laloyaux, P., Lopez, P., Lupu, C., Radnoti, G., de Rosnay, P., Rozum, I., Vamborg, F., Villaume, S., and Thépaut, J.-N.: The ERA5 global reanalysis, Q. J. Roy. Meteorol. Soc., 146, 1999–2049, https://doi.org/10.1002/qj.3803, 2020.

Holton, J. R., Haynes, P. H., McIntyre, M. E., Douglass, A. R., Rood, R. B., and Pfister, L.: Stratosphere-troposphere exchange, Rev. Geophys., 33, 403–439, https://doi.org/10.1029/95RG02097, 1995.

Huang, J. P., Fung, J. C., Lau, A. K., and Qin, Y.: Numerical simulation and process analysis of typhoon-related ozone episodes in Hong Kong, J. Geophys. Res., 110, D05301, https://doi.org/10.1029/2004JD004914, 2005.

Jöckel, P. and Ma, X.: RD1SD-base-01_Ozone, Zenodo [data set], https://doi.org/10.5281/zenodo.11093806, 2024.

Jöckel, P., Tost, H., Pozzer, A., Brühl, C., Buchholz, J., Ganzeveld, L., Hoor, P., Kerkweg, A., Lawrence, M. G., Sander, R., Steil, B., Stiller, G., Tanarhte, M., Taraborrelli, D., van Aardenne, J., and Lelieveld, J.: The atmospheric chemistry general circulation model ECHAM5/MESSy1: consistent simulation of ozone from the surface to the mesosphere, Atmos. Chem. Phys., 6, 5067–5104, https://doi.org/10.5194/acp-6-5067-2006, 2006.

Jöckel, P., Tost, H., Pozzer, A., Kunze, M., Kirner, O., Brenninkmeijer, C. A. M., Brinkop, S., Cai, D. S., Dyroff, C., Eckstein, J., Frank, F., Garny, H., Gottschaldt, K.-D., Graf, P., Grewe, V., Kerkweg, A., Kern, B., Matthes, S., Mertens, M., Meul, S., Neumaier, M., Nützel, M., Oberländer-Hayn, S., Ruhnke, R., Runde, T., Sander, R., Scharffe, D., and Zahn, A.: Earth System Chemistry integrated Modelling (ESCiMo) with the Modular Earth Submodel System (MESSy) version 2.51, Geosci. Model Dev., 9, 1153–1200, https://doi.org/10.5194/gmd-9-1153-2016, 2016.

Jöckel, P., Brinkop, S., Graf, P., Eichinger, R., Garny, H., Mertens, M., Nützel, M., and Pozzer, A.: RD1SD: EMAC CCMI-2022 hindcast simulations with specified dynamics, ERA-5, 1979–2019 (additional data), in: DOKU at DKRZ, https://www.wdc-climate.de/ui/entry?acronym=DKRZ_LTA_853_dsg0002 (last access: 13 January 2025), 2024a.

Jöckel, P., Brinkop, S., Graf, P., Eichinger, R., Garny, H., Mertens, M., Nützel, M., Pozzer, A., Tost, H., and The, M. C.: RD1SD: EMAC CCMI-2022 hindcast simulations with specified dynamics, ERA-5, 1979–2019, in: World Data Center for Climate (WDCC) at DKRZ, https://www.wdc-climate.de/ui/entry?acronym=ESCiMo2_RD1SD (last access: 13 January 2025), 2024b.

Johnson, B. J., Oltmans, S. J., Vömel, H., Smit, H. G. J., Deshler, T., and Kröger, C.: Electrochemical concentration cell (ECC) ozonesonde pump efficiency measurements and tests on the sensitivity to ozone of buffered and unbuffered ECC sensor cathode solutions, J. Geophys. Res., 107, ACH8-1–ACH8-18, https://doi.org/10.1029/2001JD000557, 2002.

Kerkweg, A., Sander, R., Tost, H., and Jöckel, P.: Technical note: Implementation of prescribed (OFFLEM), calculated (ONLEM), and pseudo-emissions (TNUDGE) of chemical species in the Modular Earth Submodel System (MESSy), Atmos. Chem. Phys., 6, 3603–3609, https://doi.org/10.5194/acp-6-3603-2006, 2006.

Konopka, P., Ploeger, F., Tao, M., Birner, T., and Riese, M.: Hemispheric asymmetries and seasonality of mean age of air in the lower stratosphere: Deep versus shallow branch of the Brewer-Dobson circulation, J. Geophys. Res.-Atmos., 120, 2053–2066, https://doi.org/10.1002/2014JD022429, 2015.

Krotkov, N. A., McLinden, C. A., Li, C., Lamsal, L. N., Celarier, E. A., Marchenko, S. V., Swartz, W. H., Bucsela, E. J., Joiner, J., Duncan, B. N., Boersma, K. F., Veefkind, J. P., Levelt, P. F., Fioletov, V. E., Dickerson, R. R., He, H., Lu, Z., and Streets, D. G.: Aura OMI observations of regional SO$_2$ and NO$_2$ pollution changes from 2005 to 2015, Atmos. Chem. Phys., 16, 4605–4629, https://doi.org/10.5194/acp-16-4605-2016, 2016.

Kunze, M., Godolt, M., Langematz, U., Grenfell, J. L., Hamann-Reinus, A., and Rauer, H.: Investigating the early Earth faint young Sun problem with a general circulation model, Planet. Space Sci., 98, 77–92, https://doi.org/10.1016/j.pss.2013.09.011, 2014.

Li, K., Jacob, D. J., Liao, H., Shen, L., Zhang, Q., and Bates, K. H.: Anthropogenic drivers of 2013–2017 trends in summer surface ozone in China, P. Natl. Acad. Sci. USA, 116, 422–427, https://doi.org/10.1073/pnas.1812168116 2019.

Liao, Z., Ling, Z., Gao, M., Sun, J., Zhao, W., Ma, P., Quan, J., and Fan, S.: Tropospheric Ozone Variability Over Hong Kong Based on Recent 20 years (2000–2019) Ozonesonde Observation, J. Geophys. Res., 126, e2020JD033054, https://doi.org/10.1029/2020JD033054, 2021.

Lin, C., Leung, K. K., Alfred, L., Tsang, R. C., Tsui, W. B., Fung, J. C., Ng, E. K., Cheung, S., Tang, A. W., and Ning, Z.: Effects of synoptic patterns on the vertical structure of ozone in Hong Kong using lidar measurement, Atmos. Environ., 257, 118490, https://doi.org/10.1016/j.atmosenv.2021.118490, 2021.

Liu, F., Zhang, Q., van der A, R. J., Zheng, B., Tong, D., Yan, L., Zheng, Y., and He, K.: Recent reduction in NOx emissions over China: synthesis of satellite observations and emission inventories, Environ. Res. Lett., 11, 114002, https://doi.org/10.1088/1748-9326/11/11/114002, 2016.

Liu, H., Jacob, D. J., Chan, L. Y., Oltmans, S. J., Bey, I., Yantosca, R. M., Harris, J. M., Duncan, B. N., and Martin, R. V.: Sources of tropospheric ozone along the Asian Pacific Rim: An analysis of ozonesonde observations, J. Geophys. Res., 107, ACH3-1–ACH3-19, https://doi.org/10.1029/2001JD002005, 2002.

Ma, Z., Xu, J., Quan, W., Zhang, Z., Lin, W., and Xu, X.: Significant increase of surface ozone at a rural site, north of eastern China, Atmos. Chem. Phys., 16, 3969–3977, https://doi.org/10.5194/acp-16-3969-2016, 2016.

Manney, G. L. and Hegglin, M. I.: Seasonal and regional variations of long-term changes in upper-tropospheric jets from reanalyses, J. Climate., 31, 423–448, https://doi.org/10.1175/JCLI-D-17-0303.1, 2018.

Meul, S., Langematz, U., Kröger, P., Oberländer-Hayn, S., and Jöckel, P.: Future changes in the stratosphere-to-troposphere

ozone mass flux and the contribution from climate change and ozone recovery, Atmos. Chem. Phys., 18, 7721–7738, https://doi.org/10.5194/acp-18-7721-2018, 2018.

Miyazaki, K., Eskes, H., Sudo, K., Boersma, K. F., Bowman, K., and Kanaya, Y.: Decadal changes in global surface NO_x emissions from multi-constituent satellite data assimilation, Atmos. Chem. Phys., 17, 807–837, https://doi.org/10.5194/acp-17-807-2017, 2017.

Monks, P. S.: A review of the observations and origins of the spring ozone maximum. Atmos. Environ., 34, 3545–3561, https://doi.org/10.1016/S1352-2310(00)00129-1, 2000.

Morgenstern, O., Hegglin, M. I., Rozanov, E., O'Connor, F. M., Abraham, N. L., Akiyoshi, H., Archibald, A. T., Bekki, S., Butchart, N., Chipperfield, M. P., Deushi, M., Dhomse, S. S., Garcia, R. R., Hardiman, S. C., Horowitz, L. W., Jöckel, P., Josse, B., Kinnison, D., Lin, M., Mancini, E., Manyin, M. E., Marchand, M., Marécal, V., Michou, M., Oman, L. D., Pitari, G., Plummer, D. A., Revell, L. E., Saint-Martin, D., Schofield, R., Stenke, A., Stone, K., Sudo, K., Tanaka, T. Y., Tilmes, S., Yamashita, Y., Yoshida, K., and Zeng, G.: Review of the global models used within phase 1 of the Chemistry–Climate Model Initiative (CCMI), Geosci. Model Dev., 10, 639–671, https://doi.org/10.5194/gmd-10-639-2017, 2017.

Morris, G. A., Labow, G., Akimoto, H., Takigawa, M., Fujiwara, M., Hasebe, F., Hirokawa, J., and Koide, T.: On the use of the correction factor with Japanese ozonesonde data, Atmos. Chem. Phys., 13, 1243–1260, https://doi.org/10.5194/acp-13-1243-2013, 2013.

Neu, J. L., Flury, T., Manney, G. L., Santee, M. L., Livesey, N. J., and Worden, J.: Tropospheric ozone variations governed by changes in stratospheric circulation, Nat. Geosci., 7, 340–344, https://doi.org/10.1038/ngeo2138, 2014.

Oltmans, S. J., Johnson, B. J., Harris, J. M., and Thompson, A. M.: Tropospheric ozone over the North Pacific from ozonesonde observations, J. Geophys. Res., 109, D15S01, https://doi.org/10.1029/2003JD003466, 2004.

Ploeger, F. and Birner, T.: Seasonal and inter-annual variability of lower stratospheric age of air spectra, Atmos. Chem. Phys., 16, 10195–10213, https://doi.org/10.5194/acp-16-10195-2016, 2016.

Plumb, R. A.: Stratospheric Transport, J. Meteorol. Soc. Jpn., 80, 793–809, https://doi.org/10.2151/jmsj.80.793, 2002.

Ray, E. A., Moore, F. L., Elkins, J. W., Dutton, G. S., Fahey, D. W., Vömel, H., Oltmans, S. J., and Rosenlof, K. H.: Transport into the northern hemisphere lowermost stratosphere revealed by in situ tracer measurements, J. Geophys. Res.-Atmos., 104, 26565–26580, https://doi.org/10.1029/1999JD900323, 1999.

Revell, L. E., Stenke, A., Tummon, F., Feinberg, A., Rozanov, E., Peter, T., Abraham, N. L., Akiyoshi, H., Archibald, A. T., Butchart, N., Deushi, M., Jöckel, P., Kinnison, D., Michou, M., Morgenstern, O., O'Connor, F. M., Oman, L. D., Pitari, G., Plummer, D. A., Schofield, R., Stone, K., Tilmes, S., Visioni, D., Yamashita, Y., and Zeng, G.: Tropospheric ozone in CCMI models and Gaussian process emulation to understand biases in the SOCOLv3 chemistry–climate model, Atmos. Chem. Phys., 18, 16155–16172, https://doi.org/10.5194/acp-18-16155-2018, 2018.

Roelofs, G.-J. and Lelieveld, J.: Model study of the influence of cross-tropopause O_3 transports on tropospheric O_3 levels, Tellus B., 49, 38–55, https://doi.org/10.3402/tellusb.v49i1.15949, 1997.

Sander, R., Baumgaertner, A., Gromov, S., Harder, H., Jöckel, P., Kerkweg, A., Kubistin, D., Regelin, E., Riede, H., Sandu, A., Taraborrelli, D., Tost, H., and Xie, Z.-Q.: The atmospheric chemistry box model CAABA/MECCA-3.0, Geosci. Model Dev., 4, 373–380, https://doi.org/10.5194/gmd-4-373-2011, 2011.

Sander, R., Jöckel, P., Kirner, O., Kunert, A. T., Landgraf, J., and Pozzer, A.: The photolysis module JVAL-14, compatible with the MESSy standard, and the JVal PreProcessor (JVPP), Geosci. Model Dev., 7, 2653–2662, https://doi.org/10.5194/gmd-7-2653-2014, 2014.

Shepherd, T. G. and McLandress, C.: A Robust Mechanism for Strengthening of the Brewer–Dobson Circulation in Response to Climate Change: Critical-Layer Control of Subtropical Wave Breaking, J. Atmos. Sci., 68, 784–797, https://doi.org/10.1175/2010JAS3608.1, 2011.

Škerlak, B., Sprenger, M., Pfahl, S., Tyrlis, E., and Wernli, H.: Tropopause folds in ERA-Interim: Global climatology and relation to extreme weather events, J. Geophys. Res., 120, 4860–4877, https://doi.org/10.1002/2014JD022787, 2015.

SPARC CCMVal: SPARC Report on the Evaluation of Chemistry Climate Models, edited by: Eyring, V., Shepherd, T. G., and Waugh, D. W., SPARC Report No. 5, WCRP-132, WMO/TD-No. 1526, http://www.sparc-climate.org/publications/sparc-reports/ (last access: 13 January 2025), 2010.

Sprenger, M., Maspoli, M. C., and Wernli, H.: Tropopause folds and cross-tropopause exchange. A global investigation based upon ECMWF analyses for the time period March 2000 to February 2001, J. Geophys. Res., 108, 8518, https://doi.org/10.1029/2002JD002587, 2003.

Stohl, A., Bonasoni, P., Cristofanelli, P., Collins, W., Feichter, J., Frank, A., Forster, C., Gerasopoulos, E., Gäggeler, H., James, P., Kentarchos, T., Kromp-Kolb, H., Krüger, B., Land, C., Meloen, J., Papayannis, A., Priller, A., Seibert, P., Sprenger, M., Roelofs, G. J., Scheel, H. E., Schnabel, C., Siegmund, P., Tobler, L., Trickl, T., Wernli, H., Wirth, V., Zanis, P., and Zerefos, C.: Stratosphere-troposphere exchange: A review, and what we have learned from STACCATO, J. Geophys. Res., 8516, https://doi.org/10.1029/2002JD002490, 2003.

Su, T., Li, J., Li, C., Xiang, P., Lau, A. K.-H., Guo, J., Yang, D., and Miao, Y.: An intercomparison of long-term planetary boundary layer heights retrieved from CALIPSO, ground-based lidar, and radiosonde measurements over Hong Kong, J. Geophys. Res., 122, 3929–3943, https://doi.org/10.1002/2016JD025937, 2017.

Sudo, K., Takahashi, M., and Akimoto, H.: Future changes in stratosphere-troposphere exchange and their impacts on future tropospheric ozone simulations, Geophys. Res. Lett., 30, 2256, https://doi.org/10.1029/2003GL018526, 2003.

Sun, L., Xue, L., Wang, T., Gao, J., Ding, A., Cooper, O. R., Lin, M., Xu, P., Wang, Z., Wang, X., Wen, L., Zhu, Y., Chen, T., Yang, L., Wang, Y., Chen, J., and Wang, W.: Significant increase of summertime ozone at Mount Tai in Central Eastern China, Atmos. Chem. Phys., 16, 10637–10650, https://doi.org/10.5194/acp-16-10637-2016, 2016.

Tost, H., Jöckel, P., Kerkweg, A., Sander, R., and Lelieveld, J.: Technical note: A new comprehensive SCAVenging submodel for

global atmospheric chemistry modelling, Atmos. Chem. Phys., 6, 565–574, https://doi.org/10.5194/acp-6-565-2006, 2006.

Tost, H., Jöckel, P., and Lelieveld, J.: Lightning and convection parameterisations – uncertainties in global modelling, Atmos. Chem. Phys., 7, 4553–4568, https://doi.org/10.5194/acp-7-4553-2007, 2007.

Trickl, T., Bärtsch-Ritter, N., Eisele, H., Furger, M., Mücke, R., Sprenger, M., and Stohl, A.: High-ozone layers in the middle and upper troposphere above Central Europe: potential import from the stratosphere along the subtropical jet stream, Atmos. Chem. Phys., 11, 9343–9366, https://doi.org/10.5194/acp-11-9343-2011, 2011.

van der A, R. J., Mijling, B., Ding, J., Koukouli, M. E., Liu, F., Li, Q., Mao, H., and Theys, N.: Cleaning up the air: effectiveness of air quality policy for SO_2 and NO_x emissions in China, Atmos. Chem. Phys., 17, 1775–1789, https://doi.org/10.5194/acp-17-1775-2017, 2017.

Verstraeten, W. W., Neu, J. L., Williams, J. E., Bowman, K. W., Worden, J. R., and Boersma, K. F.: Rapid increases in tropospheric ozone production and export from China, Nat. Geosci., 8, 690–695, https://doi.org/10.1038/NGEO2493, 2015.

Wang, T., Xue, L., Brimblecombe, P., Lam, Y. F., Li, L., and Zhang, L.: Ozone pollution in China: A review of concentrations, meteorological influences, chemical precursors, and effects, Sci. Total Environ., 575, 1582–1596, https://doi.org/10.1016/j.scitotenv.2016.10.081, 2017.

Williams, R. S., Hegglin, M. I., Kerridge, B. J., Jöckel, P., Latter, B. G., and Plummer, D. A.: Characterising the seasonal and geographical variability in tropospheric ozone, stratospheric influence and recent changes, Atmos. Chem. Phys., 19, 3589–3620, https://doi.org/10.5194/acp-19-3589-2019, 2019.

Witte, J. C., Thompson, A. M., Smit, H. G. J., Vömel, H., Posny, F., and Stübi, R.: First Reprocessing of Southern Hemisphere ADditional OZonesondes Profile Records: 3. Uncertainty in Ozone Profile and Total Column, J. Geophys. Res., 123, 3243–3268, https://doi.org/10.1002/2017JD027791, 2018.

WMO (World Meteorological Organization): Meteorology: A three dimensional science, WMO Bull, 6, 134–138, 1957.

WOUDC (World Ozone and Ultraviolet Radiation Data Centre): Ozone Sounding Dataset, Meteorological Service of Canada, Environment and Climate Change Canada, https://woudc.org/data/explore.php?lang=en (last access: 13 January 2025), 2025.

Xu, W., Lin, W., Xu, X., Tang, J., Huang, J., Wu, H., and Zhang, X.: Long-term trends of surface ozone and its influencing factors at the Mt Waliguan GAW station, China – Part 1: Overall trends and characteristics, Atmos. Chem. Phys., 16, 6191–6205, https://doi.org/10.5194/acp-16-6191-2016, 2016.

Young, P. J., Naik, V., Fiore, A. M., Gaudel, A., Guo, J., Lin, M. Y., Neu, J. L., Parrish, D. D., Rieder, H. E., Schnell, J. L., Tilmes, S., Wild, O., Zhang, L., Ziemke, J., Brandt, J., Delcloo, A., Doherty, R. M., Geels, C., Hegglin, M. I., Hu, L., Im, U., Kumar, R., Luhar, A., Murray, L., Plummer, D., Rodriguez, J., Saiz-Lopez, A., Schultz, M. G., Woodhouse, M. T., and Zeng, G.: Tropospheric Ozone Assessment Report: Assessment of global-scale model performance for global and regional ozone distributions, variability, and trends, Elem. Sci. Anth., 6, 10, https://doi.org/10.1525/elementa.265, 2018.

Zeng, G. and Pyle, J. A.: Influence of El Niño Southern Oscillation on stratosphere/troposphere exchange and the global tropospheric ozone budget, Geophys. Res. Lett., 32, L01814, https://doi.org/10.1029/2004GL021353, 2005.

Zhang, Y., Liu, H., Crawford, J. H., Considine, D. B., Chan, C., Oltmans, S. J., and Thouret, V.: Distribution, variability and sources of tropospheric ozone over south China in spring: Intensive ozonesonde measurements at five locations and modeling analysis, J. Geophys. Res., 117, D12304, https://doi.org/10.1029/2012JD017498, 2012.

Zhang, Y., Cooper, O. R., Gaudel, A., Thompson, A. M., Nédélec, P., Ogino, S.-Y., and West, J. J.: Tropospheric ozone change from 1980 to 2010 dominated by equatorward redistribution of emissions, Nat. Geosci., 9, 875–879, https://doi.org/10.1038/ngeo2827, 2016.

Zhao, K., Huang, J., Wu, Y., Yuan, Z., Wang, Y., Li, Y., Ma, X., Liu, X., Ma, W., Wang, Y., and Zhang, X.: Impact of stratospheric intrusions on ozone enhancement in the lower troposphere and implication to air quality in Hong Kong and other South China regions, J. Geophys. Res., 126, e2020JD033955, https://doi.org/10.1029/2020JD033955, 2021.

Zhou, D., Ding, A., Mao, H., Fu, C., Wang, T., Chan, L. Y., Ding, K., Zhang, Y., Liu, J., Lu, A., and Hao, N.: Impacts of the East Asian monsoon on lower tropospheric ozone over coastal South China, Environ. Res. Lett., 8, 044011, https://doi.org/10.1088/1748-9326/8/4/044011, 2013.